ISBN: 978-3-95450-208-0 doi:10.18429/JACoW-IPAC2019-WEPRB068

Ka-BAND LINEARIZER STUDIES FOR A COMPACT LIGHT SOURCE*

A. Castilla[1†], G. Burt[1], A. Latina[2], X. Liu[2], W. L. Millar[1,2], X. Wu[2], W. Wuensch[2]
[1]Lancaster University, Lancaster, UK
[2]European Organisation for Nuclear Research (CERN), Geneva, CH

Abstract

The CompactLight project is currently developing the design of a next generation hard X-ray FEL facility, based on high-gradient X-band (12 GHz) structures, bright electron photo-injectors, and compact short period undulators. However, to improve the brightness limitations due to the non- linear energy spread of the electron bunches, a Ka-band (36 GHz) linearizer is being considered to provide a harmonic compensation during the bunch compression. In this paper, we analyze the feasibility of such linearizer.

INTRODUCTION

The CompactLight (XLS) machine has different schemes under study, both the science requirements and the facility design options are discussed in [1, 2]. The machine layout under study in this paper, requires a 36 GHz linearizer that can provide up to 25 MV of integrated longitudinal voltage, to correct for the bunch energy spread. Therefore the scope of this manuscript centres on determining the feasibility for such a structure, from the view point of the available rf power [3], and the final structure length necessary to provide the given voltages at such frequency.

SINGLE CELL DESIGN

We start by exploring the parameter space of the single cell geometry. For this, we have selected 2 main cell geometries, a simple and a reentrant cell, depicted in Fig. 1 as (**1**) and (**2**), respectively. For each one of these two geometries we scanned three different variations: non curved edges, single curved edge, and double curved edges, also shown in Fig. 1 as (**a**), (**b**), and (**c**), respectively.

After exploring the parameter space for each of the geometries, it was determined that for both cases: simple (**1**) and reentrant (**2**), the most promising variants corresponded to the double bend edges case (**c**). Therefore, to illustrate the optimization process, we will only compare the rf properties of these configurations, as a function of the iris aperture for each phase advance (120° and 150°), as shown in Figs. 2 and 3.

Figure 2 shows that while the phase advance does not reflects on a considerable difference for the shunt impedance, it has a slight improvement on the intrinsic Q-factor (top) with the aperture, and that the attenuation factor is comparable between both phase advances at around 22-m iris radius and above (bottom), for a given iris aperture, in the case of the simple geometry.

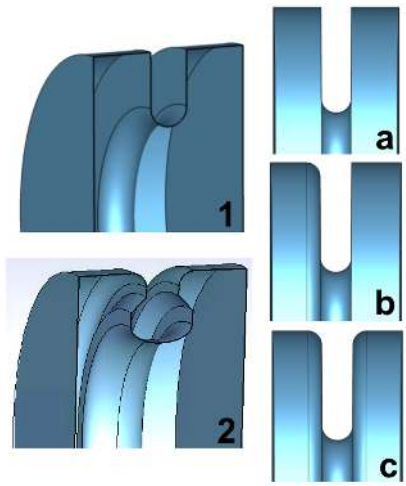

Figure 1: Sketches of the simple (**1**) and reentrant (**2**) single cell geometries, and their non (**a**), single (**b**), and double (**c**) curved edges variations.

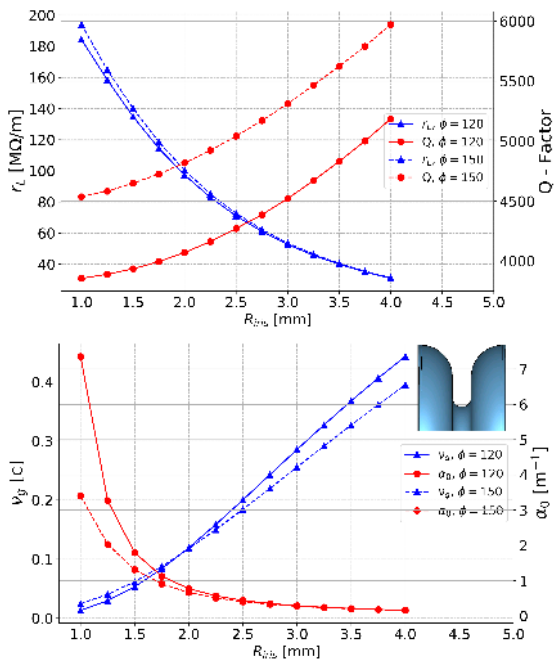

Figure 2: Plots of the shunt impedance and Q-factor (top), group velocity and attenuation factor (bottom) of the simple double bend geometry as a function of the iris aperture.

Figure 3 shows for the reentrant cell, that the shunt impedance follows a similar trend as for the simple cell, but in this case the 120° and the 150° variations can easily

* Founded by the European Union's Horizon 2020 research and innovation program under Grant Agreement No. 777431.
† a.castilla@cern.ch

ISBN: 978-3-95450-208-0 doi:10.18429/JACoW-IPAC2019-WEPRB068

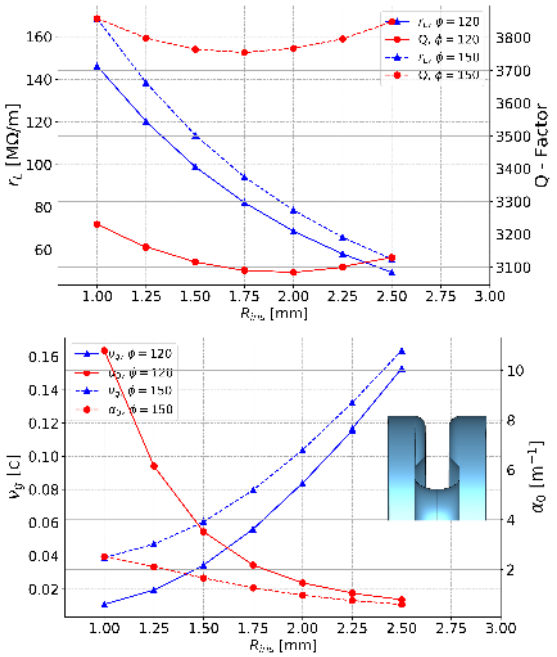

Figure 3: Plots of the shunt impedance and Q-factor (top), group velocity and attenuation factor (bottom) of the reentrant double bend geometry as a function of the iris aperture.

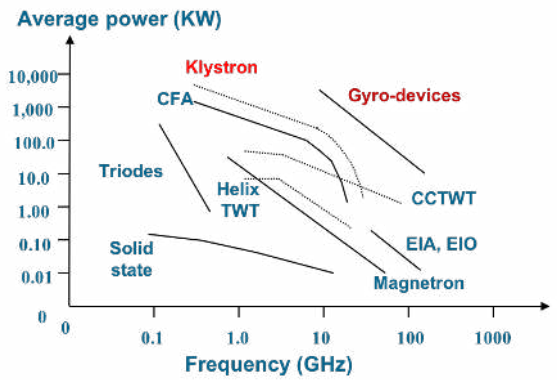

Figure 4: Typical performance of rf souces as a function of frequency [3].

be distinguished from each other (by 13%). The rest of the significant figures also show similar behaviour to those described in Fig. 2. However, is interesting to note how the intrinsic Q-factor shows a minimum at around an iris radius of 1.75 mm, and that for 150° phase advance, the attenuation factor is considerably lower at apertures below 2 mm, while both phase advances are comparable above this iris radius, being the 150° variant the one showing better overall performance for a given iris radius aperture.

POWER AVAILABILITY

Figure 4 shows the expected performance for different state of the art rf sources as a function of the operating rf frequency. The University of Strathclyde has been developing gyro-klystron sources that could provide 2-µs pulses of up

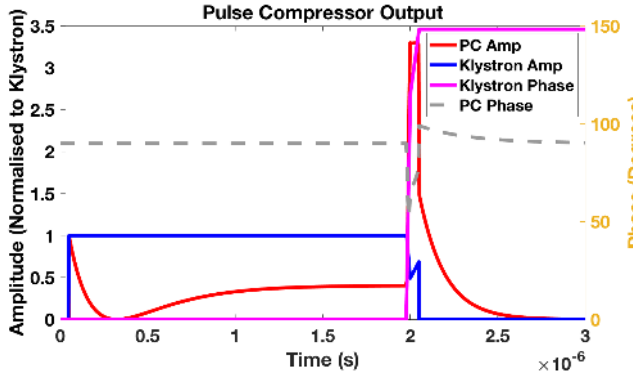

Figure 5: Simulated response of a SLEDI pulse compressor.

to 3 MW flat top at 36 GHz [3], which provides the structure under study in this paper with promising operating options.

Even when Strathclyde's gyro-klystron option, 3 MW may not be sufficient to reach the desirable gains in the linearizer, which implies the need for a pulse compressor. Figure 5 shows a simulated response of a SLEDI pulse compressor (red), to a square 2 µs pulse (blue) and a programmed phase ramp (pink). The left hand axis shows the power normalized to the klystron output.

A pulse compressor as the SLEDI es capable of providing 50-ns compressed pulses with a gain of up to four times the klystron output power, which gives a comfortable margin for the operation of the linearizer. There are two important things to point out with this respect: the first one refers to the fact that since the FEL operates with a single bunch scheme, there is no need for a flat top on the compressed pulse, so we do not actually need the programmed phase ramp. The second important thing to mention is that having a SLEDI pulse compressor for this application raises the question of efficiency, since the intrinsic Q-factors of the cavities decreases with the frequency, it is unlikely to get sufficient gains out of a cavity-based pulse compressor. However, using a delay line should avoid this difficulty, making the SLEDII pulse compressor a better choice.

SHORT RANGE WAKEFIELDS

For a single bunch machine, and having structures with such small apertures, the short range wakefields play an important role on he longitudinal beam dynamics. Analytical and numerical calculations of the effects of the wakefields, based on the structure geometry have been used in the past [4]. In a similar fashion, Fig. 6 shows the bunch energy modulation due to the longitudinal wakefields (top) and the transverse kick seen by the bunch due to the short range transverse wakefields with a 10 and 15% of σ_y jitter, respectively (bottom), calculated using the parameters described in Table 1 [5].

PERFORMANCE AND CONCLUSIONS

We now calculate the integrated voltages reached by a 1-m long traveling wave structure for different input powers, as a

ISBN: 978-3-95450-208-0 doi:10.18429/JACoW-IPAC2019-WEPRB068

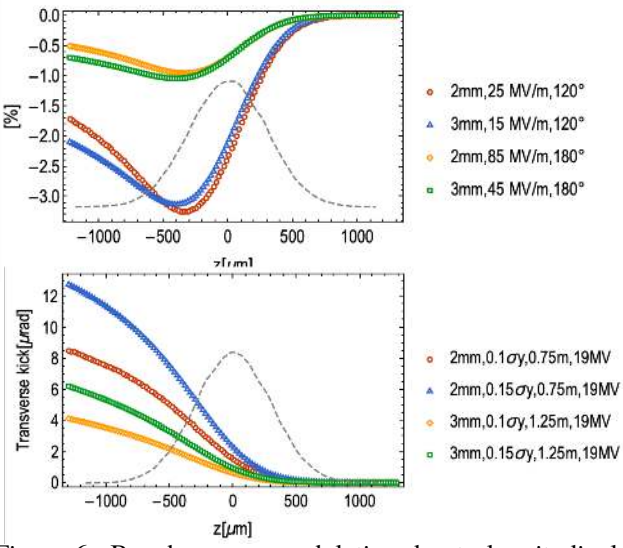

Figure 6: Bunch energy modulation due to longitudinal wakefields (top) and transverse kick due to short range transverse wakefields for a jitter of 10% and 15% on σ_y.

Table 1: Wakefield Simulation Parameters

Parameter	Value	Units
$< \beta_y >$	6	m
$\epsilon_{x,y}$	0.4	μm
E	230	MeV
σ_z	300	μm
Q	0.4	μm
N	100,000	- -
$\sigma\,(\delta)$	0.03	%

function of the iris aperture. Using the conclusions drawn in the single cell design section, we limit our comparison to the simple cell in a $2\pi/3$ mode and the reentrant cell ina $5\pi/6$ mode, each with the double bend edges (see Fig. 7).

Taking into account the arguments discussed in the previous sections, we can consider with confidence a 50 ns flat top of 8 MW as a comfortable working point for the available rf power. While, from the wakefields view point, a 2-mm iris radius represents a reasonable working point. Then both geometry variants show similar performance at this aperture, as shown in Fig. 7. Therefore a simple geometry is preferred over a reentrant cell, due to that it makes for an easier–and therefore cheaper—manufacture, with similar performance.

Finally, we propose a simple single cell geometry with symmetrically rounded edges and 120° phase advance, for a 1-m traveling wave structure as baseline for the linearizer. Figure 8 shows a diagrammatic description of the geometry design, while Table 2 lists the parameters of the proposed design.

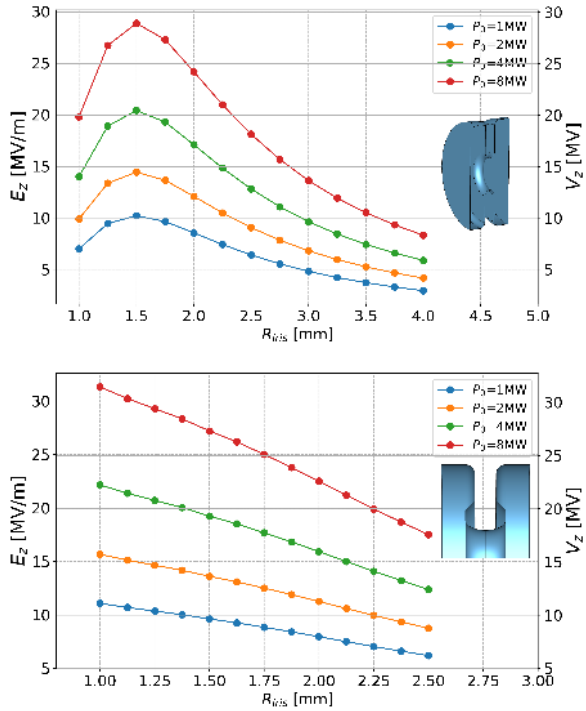

Figure 7: Integrated voltage for different input powers ,as a function of the iris aperture for the simple double blends and 120° phase advance (top), and for the reentrant double bends and 150° phase advance (bottom).

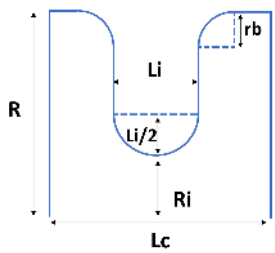

Figure 8: Single cell geometry diagram.

Table 2: Proposed Single-Cell Parameters

Parameter	Value	Units
f	36	GHz
Q	4392	- -
r_L	106	MΩ / m
ν_g	0.12	c
α_0	0.7	m$^-$1
E_p^*	2.6	MV/m
R	3.96	mm
R_i	2.00	mm
L_c $(\phi = 2\pi/3)$	2.78	mm
L_i	0.60	mm
r_b	1.00	mm

*norm. to E_z = 1MV/m

ISBN: 978-3-95450-208-0 doi:10.18429/JACoW-IPAC2019-WEPRB068

REFERENCES

[1] XLS Deliverable D2.1, FEL science requirements and facility design, https://www.compactlight.eu/uploads/Main/D2.1_XLS_Specification.pdf

[2] A. Aksoy, "WP6 activity report", presented at *First XLS - CompactLight Annual Meeting*, Barcelona, Spain, Dec. 2018, https://indico.cern.ch/event/779185/contributions/3245341/attachments/1768845/2873840/XLS_WP6_progress_11-12-2018_a_aksoy.pdf

[3] W. He *et al.*, "Update on the 36-GHz and 48-GHz power sources", presented at *First XLS - CompactLight Annual Meeting*, Barcelona, Spain, Dec. 2018, https://indico.cern.ch/event/779185/contributions/3245341/attachments/1768845/2873840/XLS_WP6_progress_11-12-2018_a_aksoy.pdf

[4] K. Bane, "Short-range dipole wakefields in accelerating structures for the NLC", Technical Note LCC-0116, SLAC-PUB-9663, Mar. 2003.

[5] X. Liu and A. Latina, "Longitudinal design considerations", presented at *First XLS - CompactLight Annual Meeting*, Barcelona, Spain, Dec. 2018, https://indico.cern.ch/event/779185/contributions/3245355/attachments/1769007/2874740/WP6-1stAnnualMeeting-Barcelona-Liu.pdf